Progress In Electromagnetics Research, Vol. 127, 479–499, 2012

NON LINEAR OPTIMIZATION TECHNIQUE FOR THE REDUCTION OF THE FREQUENCY SCANNING EFFECT IN A PHASED ARRAY BASED ON BROADBAND INJECTION-LOCKED THIRD HARMONIC SELF-OSCILLATING MIXERS

M. Fernandez*, S. Ver Hoeye, C. Vazquez, G. Hotopan, R. Camblor, and F. Las Heras

Area of Signal Theory and Communications, Department of Electrical Engineering, University of Oviedo, Campus de Viesques, Edificio Polivalente s/n, Modulo 8, Planta 1, Gijon E-33203, Spain

Abstract—In this work, an electronically tunable large range phase shifter based on a broadband Injection-Locked Third Harmonic Self-Oscillating Mixer (IL3HSOM) is designed and analyzed. This multi-functional circuit generates a down-converted Intermediate Frequency (IF) signal and provides a theoretical 540° continuous phase shift range. The conversion gain and the bandwidth of the circuit are optimized through bifurcation control techniques. The IL3HSOM will be used as the core of a broadband phased antenna array with electronic beam-steering capabilities. The use of a multi-harmonic load based on an arbitrarily width modulated transmission line allows the nonlinear optimization of the circuit phase shift frequency response to compensate the *frequency scanning* effect, which negatively influences the performance of broadband antenna arrays.

1. INTRODUCTION

For the design of antenna arrays with electronic beam-steering capabilities [1–3], low cost phase shifter circuits are required to control the phase distribution along the array. During the last few years, different approaches for the implementation of phase shifters have been proposed. On the one hand, digital phase shifters based on switching devices such as PIN diodes [4] or MEMS [5] have been developed. The main drawbacks of these devices are the phase error due to

Received 6 February 2012, Accepted 17 April 2012, Scheduled 7 May 2012
* Corresponding author: Miguel Fernandez (Garcia mfgarcia@tsc.uniovi.es).

the discrete operation and the phase shift dependent insertion losses. Other approaches for the implementation of analog phase shifters based on ferrite components [6] and passive coupled-line structures [7] have also been described. These devices are unsuitable for the design of low cost planar arrays because of their heavy weight and large size, and the difficulty to be integrated with planar structures.

On the other hand, analog large range phase shifters based on injection-locked oscillators have been described [8–11]. In this case the phase error is completely prevented. In addition, these multifunctional circuits provide several key advantages such as their reduced size, low cost and power consumption, since, with a single transistor and a reduced number of components, several blocks of the communication system can be implemented: electronically tunable continuous range phase shifting, first low noise amplification stage, frequency down-conversion and local oscillator signal generation.

The maximum phase shift range that can be obtained when the oscillator is injection-locked at the fundamental harmonic component of the autonomous signal is limited to 180° [8–10]. This range can be extended up to 360° using double stage designs [11]. In both cases, these theoretical ranges are further reduced due to the strong noise amplification effect which occurs when the circuit works at the limits of the synchronization range [12].

In this work, a variable large range phase shifter based on an Injection-Locked Third Harmonic Self-Oscillating Mixer (IL3HSOM) is analyzed and optimized. The circuit provides a theoretical phase shift range of 540° [13], which ensures a usable range of, at least 360°. The conversion gain and the bandwidth of the IL3HSOM will be enhanced through a technique based on bifurcation control theory [14].

The IL3HSOM based phase shifter will be applied in the design of a wide band active phased antenna array. Due to the broadband operation of the system, the undesired variation of the steering angle with the frequency, known as *frequency scanning* effect, must be taken into account. The optimum IL3HSOM phase shift frequency response, which depends on the particular considered array, will be calculated and imposed to the phase shifter in order to reduce the impact of the frequency scanning effect on the array performance.

This paper is organized as follows: In Section 2, the topology and the design process of the IL3HSOM are presented. In addition, the technique used in order to increase the conversion gain and the bandwidth of the circuit is briefly described. Section 3 is devoted to the analysis of the synchronized solutions through a technique based on the use of an auxiliary generator. The stability of such solutions is determined by means of the Envelope Transient technique. Finally, the

application of the phase shifter to the desing of a broadband phased array is described in Section 4, focusing on the optimization of the phase shift frequency response to reduce the frequency scanning effect.

2. DESIGN AND OPTIMIZATION OF THE IL3HSOM

2.1. Topology

The topology of the circuit is represented in Fig. 1. The IL3HSOM is based on a single ultra low noise PHEMT transistor with a feedback network placed at the source terminal, which provides the negative resistance required at the gate port for the start-up of the autonomous signal, with frequency $f_o = 3.25\,\text{GHz}$, amplitude V_o and phase ϕ_o. The feedback network includes a varactor which will be used to electronically adjust the phase shift provided by the circuit. The input RF signal, with center frequency $f_{\text{RF}} = 11\,\text{GHz}$ and power P_{RF} is connected to the gate port through a band-pass filter. The input reference signal, with frequency $f_{\text{ref}} = f_o$, power P_{ref} and phase ϕ_{ref} is connected to the gate port through another band-pass filter, with center frequency f_{ref}. A multi-harmonic load based on an arbitrarily width modulated transmission line [15] is also connected to the gate port of the transistor. The parameters of this load will be used along the entire design and optimization process. The output IF signal, with center frequency $f_{\text{IF}} = f_{\text{RF}} - 3f_o = 1.25\,\text{GHz}$ is obtained through a mixing operation between the input RF signal and the third harmonic component of the autonomous signal. This output signal is selected at the drain port of the transistor by means of a band-pass filter. The auxiliary generator, connected at the gate port of the transistor, will be used for analysis and optimization purposes.

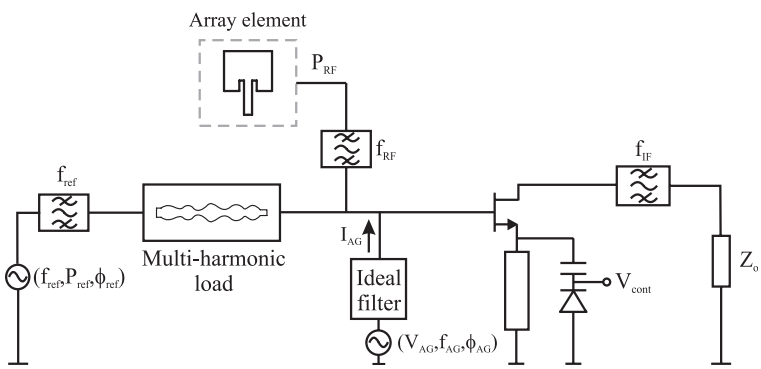

Figure 1. Topology of the injection-locked third harmonic self-oscillating mixer.

2.2. Autonomous Solution

Due to the limitations of the oscillator design linear methods [16], in this work, the auxiliary generator technique is used to set the autonomous solution of the IL3HSOM [13, 14, 17]. The auxiliary generator is connected to the gate port of the transistor and works with frequency $f_{AG} = f_o$, amplitude $V_{AG} = V_o$ and phase ϕ_{AG}. The frequency f_o and the amplitude V_o of the fundamental harmonic component of the autonomous signal are imposed through an optimization process in which several parameters of the circuit, including those of the multi-harmonic load, are modified in order to satisfy the non-perturbation condition of the auxiliary generator $Y_{AG} = I_{AG}/V_{AG} = 0$ [13], expressed in terms of its real and imaginary parts as:

$$\begin{cases} Y^r_{AG}(f_{AG} = f_o,\ V_{AG} = V_o,\ \ \phi_{AG} = \phi_o,\ \ \bar{\gamma}_p) = 0 \\ Y^i_{AG}(f_{AG} = f_o,\ V_{AG} = V_o,\ \ \phi_{AG} = \phi_o,\ \ \bar{\gamma}_p) = 0 \end{cases} \tag{1}$$

where the superscripts $(^r)$ and $(^i)$ are used to denote the real and imaginary parts, respectively, and $\bar{\gamma}_p$ represents the set of optimization variables. When this condition is fulfilled, the current through the auxiliary generator is zero. Therefore, no power is dissipated by or delivered to the circuit, which means that the circuit is able to maintain the autonomous signal.

2.3. Optimization of the Conversion Gain and Bandwidth

The auxiliary generator technique allows an accurate control over the frequency f_o and the amplitude V_o of the autonomous signal. However, it cannot deal with the traditional limitations of Harmonic Self-Oscillating Mixer (HSOM) based circuits, namely, the high conversion losses and the narrow bandwidth of the mixing operation. In this work, the conversion gain and the bandwidth of the IL3HSOM will be considerably enhanced through the application of a recently described technique, which enables the independent control of the harmonic content and the working regime of the circuit [14, 18].

Since the third harmonic component of the autonomous signal is used as local oscillator signal, its amplitude V_o^3 is expected to have a great influence on the IL3HSOM conversion gain. In addition, due to the autonomous nature of the circuit, the amplitude of the fundamental harmonic component of the self-oscillation signal also determines its overall behavior. The values of V_o and V_o^3 are easily imposed to the circuit through the auxiliary generator technique, which makes possible the analysis of the influence of the pair $(V_o,\ V_o^3)$ on the conversion gain.

The maximum conversion gain that can be reached with this method is about $G_c \approx -20\,\text{dB}$.

The conversion gain is considerably improved through the application of a technique which takes advantage of the strong amplification effect which is generated when the working regime of a non linear circuit is close to a Hopf bifurcation point [12]. This phenomenon will be used to amplify the input RF signal before the mixing operation [14, 18]. In this case, the operation regime of the circuit will be forced to be near three Hopf bifurcation points, distributed along the input frequency band, in order to combine the amplification effect associated with each of them.

The frequency response of the conversion gain, achieved after setting the desired operation regime, is represented in Fig. 2. Note that, due to the adequate selection of the harmonic content of the autonomous signal and the circuit operation regime, the conversion gain provided by the IL3HSOM is about $G_c \approx 3\,\text{dB}$ over a 1 GHz bandwidth, and exhibits very low ripple.

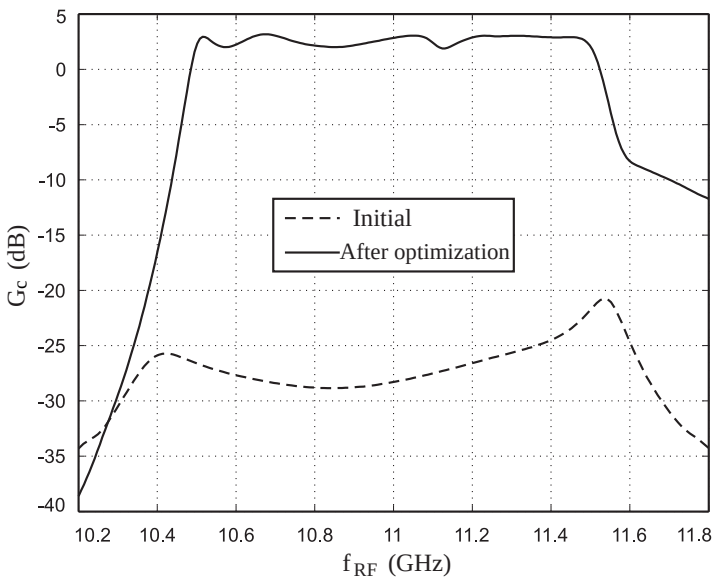

Figure 2. Conversion gain of the IL3HSOM. Dashed line: Initial conversion gain, with $V_o = 1.1\,\text{V}$ and $V_o^3 = 25\,\text{mV}$. Continuous line: Conversion gain after setting the operation regime close to three Hopf bifurcation points.

3. ANALYSIS OF THE SYNCHRONIZED SOLUTIONS

In synchronized operation, the frequency of the autonomous signal is modified to be equal to that of the input reference signal $f_o = f_{\text{ref}}$, and the phase difference between them, expressed as $\Delta\phi = \phi_o - \phi_{\text{ref}}$, is constant in time. The value of $\Delta\phi$ is given by the well known Adler equation [19]:

$$\sin(\Delta\phi) = 2Q\frac{\Delta f_o}{f_o}\sqrt{\frac{P_o}{P_{\text{ref}}}} \tag{2}$$

where Q is the quality factor of the circuit, P_o is the power of the autonomous signal and $\Delta f_o = f_o - f_{\text{ref}}$. Since the frequency of the reference signal is constant, the phase shift $\Delta\phi$ provided by the IL3HSOM can be controlled by modifying the natural self-oscillation frequency f_o, through the control of the DC voltage signal applied to the varactor. Due to the fact that $-1 \leq \sin(\Delta\phi) \leq 1$, the maximum value of $\Delta\phi$ is limited to 180°. Therefore, the maximum phase change of the third harmonic component of the autonomous signal is 540°.

The synchronized solutions are obtained by sweeping $\Delta\phi = \phi_o - \phi_{\text{ref}}$ between 0° and 360°. At each point of the sweep, the values of V_o and the varactor capacity C_{var} for which the non-perturbation condition of the auxiliary generator is fulfilled, are recalculated [13, 14]. Since ϕ_{ref} represents the phase of the reference signal, it can be arbitrarily set to $\phi_{\text{ref}} = 0°$. Therefore, the synchronized solutions can be found by sweeping the phase of the auxiliary generator, since $\Delta\phi = \phi_o = \phi_{AG}$.

Figure 3(a) shows the obtained synchronization loci, for different values of the reference signal power P_{ref}, in terms of the amplitude of the autonomous signal V_o and the varactor capacity C_{var} associated with each phase shift point $\Delta\phi = \phi_{AG}$. The reached phase shift, calculated at the frequency of the fundamental harmonic component of the autonomous signal, is represented versus C_{var} in Fig. 3(b). Note that the maximum phase shift range does not depend on the power of the reference signal P_{ref}. However, the varactor capacity variation required in order to achieve a particular phase shift value increases with P_{ref}. The phase shift evaluated at the intermediate frequency signal, at the output port, is represented in Fig. 4. This signal is obtained from the third harmonic component of the autonomous signal, as $f_{\text{IF}} = f_{\text{RF}} - 3f_o$. Thus, the maximum phase shift that can be achieved is $\Delta\phi_{\text{IF}} = 3\Delta\phi$. Notice that, in Figs. 3(b) and 4, there is a value of C_{var} for which the phase shift does not depend on the reference signal power P_{ref}. The output network of the circuit has been designed in order to ensure that such point is associated to an IF phase shift $\Delta\phi_{\text{IF}} = 0°$.

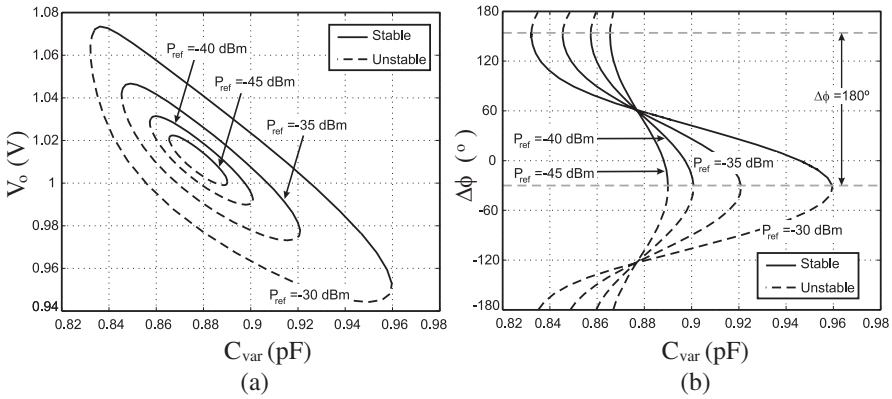

(a) (b)

Figure 3. Synchronized solutions for different values of P_{ref}. (a) Amplitude of the autonomous signal. (b) Phase shift evaluated at the fundamental harmonic component of the autonomous signal. Continuous line: Stable solutions. Dashed line: Unstable solutions.

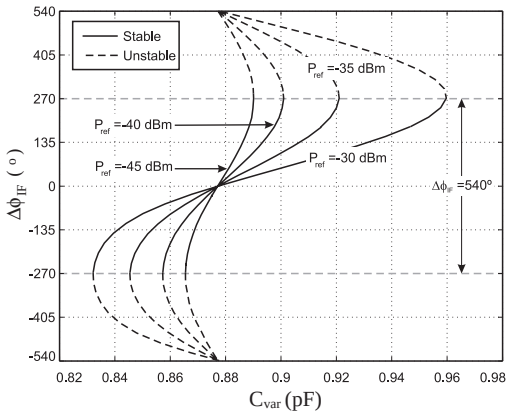

Figure 4. Phase shift evaluated at the IF signal, for different values of P_{ref}. Continuous line: Stable solutions. Dashed line: Unstable solutions.

Since the synchronized solutions represented in Figs. 3 and 4 have been calculated using the Harmonic Balance technique, they are steady-state solutions. As can be observed, for each value of C_{var}, there are two possible synchronized solutions. However, only one of them is stable and physically observable. Therefore, the maximum reachable stable phase shift is limited to 180° in the case of the fundamental harmonic component of the autonomous signal, and 540° in the case of the IF signal, instead of the represented 360° and 1080° ranges, respectively. The stability of the synchronized solutions has

been analyzed by using the Envelope Transient technique in order to determine the temporal evolution of the circuit state variables [17]. In Figs. 3 and 4, the stable synchronized solutions have been represented with continuous trace, while the unstable ones are depicted with dashed line.

3.1. Conversion Gain Along the Synchronization Loci

The influence of the reference signal power P_{ref} and the working point of the IL3HSOM along the synchronization loci on the conversion gain has been analyzed. On the one hand, the impact of the working point on the conversion gain, calculated at the center frequency of the working band $f_{\text{RF}} = 11\,\text{GHz}$, has been represented in Fig. 5(a). The maximum variation is about 0.8 dB when $P_{\text{ref}} = -30\,\text{dBm}$. This variation is considerably reduced in the case of $P_{\text{ref}} = -40\,\text{dBm}$, and negligible for lower reference signal power values. It must be taken into account that only stable solutions are considered in this analysis.

On the other hand, the variation of the conversion gain along the working band has also been characterized. The difference $\Delta G_c = G_{c,\,2} - G_{c,\,1}$ between the conversion gain evaluated at the limits of the locking range, $G_{c,\,1}$ and $G_{c,\,2}$, has been depicted in Fig. 5(b). As in the previous analysis, the variation of the conversion gain increases with P_{ref}. This is due to the fact that, for growing values of P_{ref}, the varactor capacity variation C_{var} must be greater in order to reach a particular phase shift $\Delta\phi_{\text{IF}}$. Note that, for $P_{\text{ref}} = -40\,\text{dBm}$, the maximum ripple is about 1 dB.

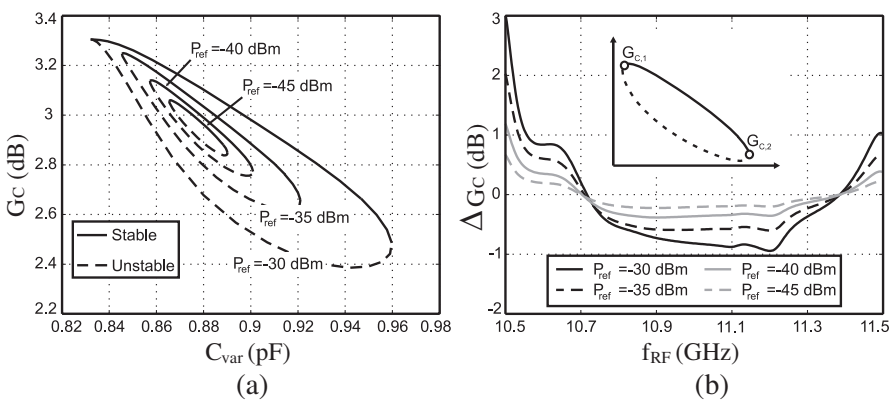

Figure 5. (a) Conversion gain, evaluated at $f_{\text{RF}} = 11\,\text{GHz}$, along the synchronization loci. Stable solutions are represented with continuous line. (b) Difference between the conversion gain evaluated at the limits of the locking range $\Delta G_c = G_{c,\,2} - G_{c,\,1}$.

From the data represented in Fig. 5, the adequate reference signal power P_{ref} and the varactor diode for each particular application can be selected, depending on the maximum allowable variation of the conversion gain. It must be taken into account that the theoretical maximum phase shift does not depend on P_{ref}, but its value determines the sensitivity of $\Delta\phi_{\text{IF}}$ to C_{var} and, therefore, to the DC control signal.

4. BROADBAND ANTENNA ARRAY BASED ON IL3HSOM

In this section, the use of broadband high gain variable phase shifters on a 4×1 active antenna array and the optimization of the circuit frequency response will be described.

4.1. Topology of the Array

The topology of the active array is shown in Fig. 6(a). The system is based on four identical IL3HSOM circuits. The input RF signal of each one is provided by one of the four radiating elements which compose the antenna array. The reference signal is connected to the IL3HSOM circuits through a Wilkinson power divider, which is designed to ensure that the power P_{ref} and the phase ϕ_{ref} are the same for the four phase shifters. The system output IF signal is obtained by combining the output IF signals of each IL3HSOM. The use of band-pass filters at all ports of the phase shifters avoids the mutual coupling between them through the harmonic components of their autonomous signals.

In order to generate a feeding distribution with constant amplitude and progressive phase shift ϕ_p, the operating points of the four IL3HSOM circuits must be distributed along the synchronization loci as indicated in Fig. 6(b), where ϕ_p represents the progressive phase difference between two adjacent circuits of the system. The value of ϕ_p determines the beam-steering angle θ_m of the antenna, and can be modified by means of the DC control signals which are applied to the varactors. Note that ϕ_p is evaluated at the output IF signal of the IL3HSOMs. Hence, its maximum value is limited to 180°.

The base elements of the array are square patch antennas [20, 21]. This radiating element has been selected due to its low profile, compactness, lightness, low cost and the possibility of integrating them together with the phase shifters [22], or with other circuitry [23], in the same substrate. The patch antennas are fed through electromagnetic coupling [24], in order to enlarge their bandwidth without requiring additional parasitic elements [25, 26] or using more complex design techniques [27].

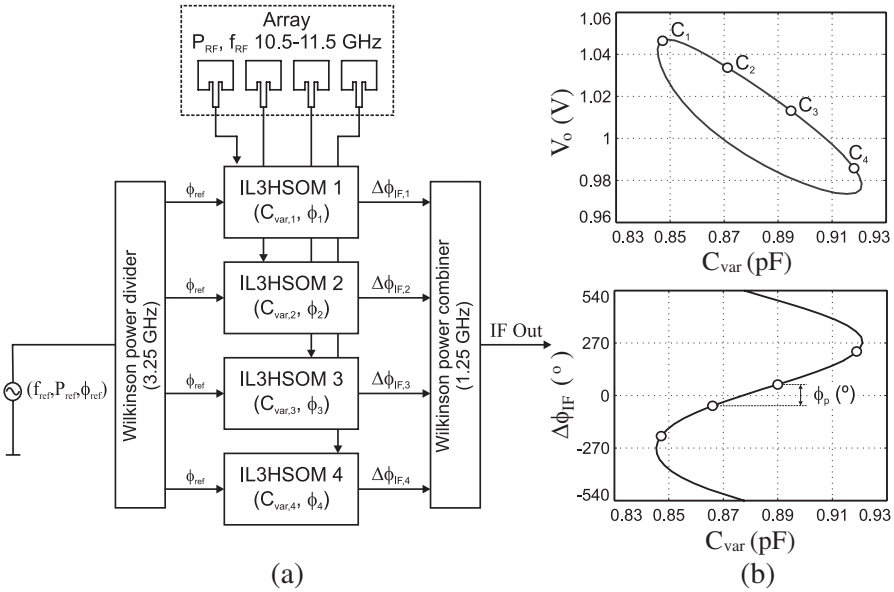

Figure 6. (a) Topology of the active phased array. (b) Operating points of the four circuits along the synchronization loci (top) and phase shift evaluated at the IF signal (bottom).

4.2. Frequency Scanning Effect

From the antenna array theory, in a linear array composed of low directivity individual elements, the beam-steering angle θ_m is given by:

$$\theta_m = \arcsin\left(-\frac{\phi_p}{kd}\right) \tag{3}$$

where d is the distance between adjacent radiating elements and $k = 2\pi/\lambda = 2\pi/cf$. As will be seen below, the value of ϕ_p remains practically constant over the whole considered frequency band, from $f_{\mathrm{RF}} = 10.5\,\mathrm{GHz}$ to $f_{\mathrm{RF}} = 11.5\,\mathrm{GHz}$. Therefore, the beam-steering angle of the array will change with the frequency of the input RF signal, because of the frequency dependence of the term k in (3), leading to the frequency scanning effect. Note that the magnitude of this effect increases with the value of ϕ_p and with the system bandwidth. Thus, it is specially relevant when using high directivity antennas in broadband applications.

Since the radiation pattern of the antenna array depends on the array factor and the radiation pattern of the base element, the patch antenna array has been completely characterized through

electromagnetic simulations based on the Method of Moments [28]. The influence of the input RF signal frequency on the angle θ_m for which the maximum gain is reached has been analyzed and represented in Fig. 7, with respect to $\theta_{m,c}$, which represents the value obtained at the center frequency $f_{\mathrm{RF}} = 11\,\mathrm{GHz}$. The inset shows the beam-steering angle $\theta_{m,c}$ versus ϕ_p, evaluated at $f_{\mathrm{RF}} = 11\,\mathrm{GHz}$.

As can be derived from (3), the variation of θ_m versus the frequency increases with ϕ_p. Note that the variation of θ_m with the frequency represented in Fig. 7 does not match the behavior predicted by (3) due to the particular characteristics of the radiation pattern of the array base element. Therefore, the influence of the frequency scanning effect on the angle θ_m depends on the array considered in each case. For the sake of representation clarity, negative values of ϕ_p are not considered.

4.3. Optimum Frequency Response

The optimum frequency response of $\phi_p \equiv \phi_p(f)$ could be obtained from (3) and expressed as:

$$\phi_p\,(f) = -kd\sin(\theta_{m,c}) = -\frac{2\pi}{c} f d \sin(\theta_{m,c}) \tag{4}$$

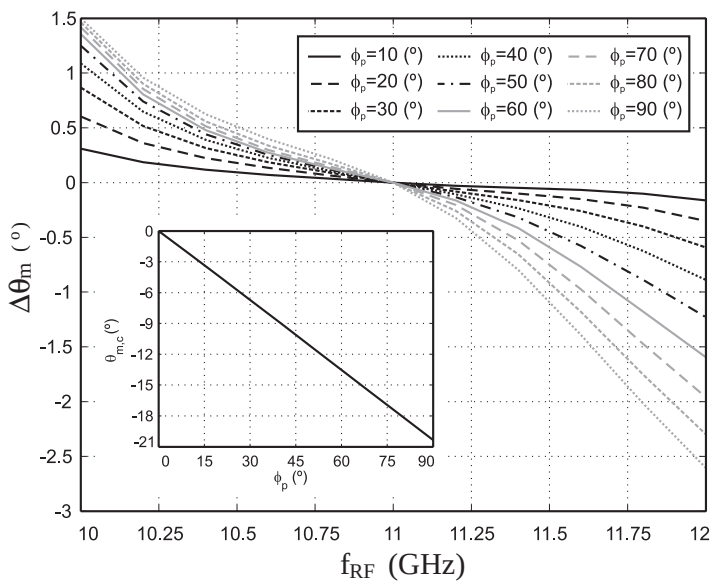

Figure 7. Frequency scanning effect evaluated over the real antenna array. Inset: $\theta_{m,c}$ versus ϕ_p ($f = 11\,\mathrm{GHz}$).

However, since the theoretical array behavior indicated in (3) does not match that of the real antenna, represented in Fig. 7, the analytically calculated frequency response given by (4) cannot be used in order to prevent the frequency scanning effect.

The real and the theoretical values of the frequency dependent beam-steering angle θ_m have been represented in Fig. 8(a), for different values of the progressive phase shift ϕ_p. Although the maximum reachable ϕ_p value is 180° (see Fig. 6(b)) and Fig. 8(a) shows θ_m variation up to $\phi_p = 110°$, when $\phi_p > 90°$, the side lobes of the array radiation pattern are greater than $-10\,\text{dB}$. Therefore, $\phi_p = 90°$ is the maximum considered value.

In order to empirically determine the optimum frequency response of ϕ_p, the considered frequency band is discretized into a finite number of frequency points $f_i \in [10,\ 12]\,\text{GHz}$. For each frequency point f_i, the value of the beam-steering angle $\theta_{m,\,f_i}(\phi_p)$, which depends on ϕ_p, is extracted. The collected data has been represented in Fig. 8(b). Note that, for each frequency point f_i, the dependence of $\theta_{m,\,f_i}(\phi_p)$ with ϕ_p is almost linear. Hence, the angle for which maximum gain is achieved, at frequency f_i, can be expressed as a function of ϕ_p as:

$$f_i \rightarrow \theta_{m,\,f_i} \approx \alpha_{f_i}\phi_{p,\,f_i} + \beta_{f_i} \tag{5}$$

where the frequency dependent coefficients α_{f_i} and β_{f_i} have been calculated by least mean squares fitting. From (5), the value of the progressive phase shift $\phi_{p,\,f_i}$ required in order to reach a beam-steering

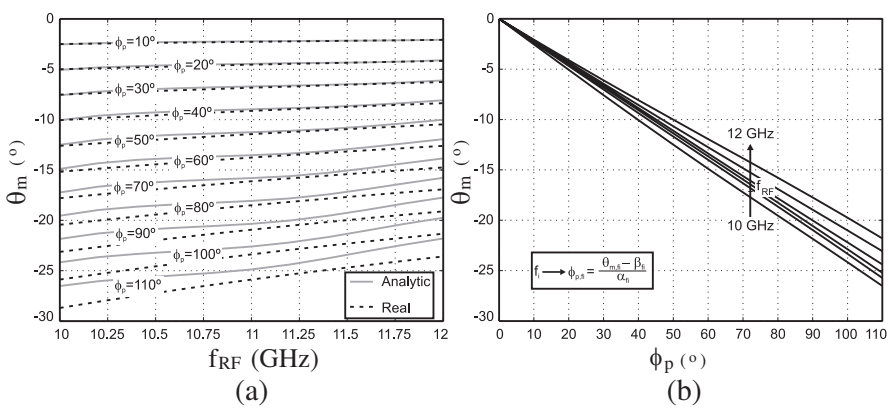

Figure 8. (a) Dependence of θ_m with the frequency of the input RF signal. Continuous line: Real variation, calculated through electromagnetic simulations. Dashed line: Theoretical variation due to the array factor, given by (3). (b) Variation of θ_m versus ϕ_p, evaluated for several frequency points f_i.

angle $\theta_{m,\,f_i}$ at frequency f_i, can be directly obtained:

$$\phi_{p,\,f_i} \approx \frac{\theta_{m,\,f_i} - \beta_{f_i}}{\alpha_{f_i}} \tag{6}$$

The optimum frequency response of the progressive phase shift $\phi_p \equiv \phi_p(f,\,\theta_{m,\,c})$ is achieved by repeating the described procedure for all the considered frequency points $f_i \in [10,\,12]$ GHz. The obtained results have been represented in Fig. 9. Note that the frequency response of ϕ_p depends on the the value of $\theta_{m,\,c}$.

4.4. Optimization of the Phase Shifter Frequency Response

From Fig. 9, it can be observed that the frequency response of ϕ_p depends on the beam-steering angle $\theta_{m,\,c}$, evaluated at the center of the frequency band. The intermediate case, obtained when $\theta_{m,\,c} = -10°$ has been selected to be imposed to the IL3HSOM circuit.

Since the working points of the four IL3HSOM circuits in the system are distributed along the synchronization loci as indicated in Fig. 6(b), the frequency response of the phase shift $\phi_p(f)$ can be calculated as the difference between the output IF signal phase $\Delta\phi_{\mathrm{IF}}$ of two adjacent circuits. This difference is represented by the variable set $\phi_{p,\,i}(f)$, with $i = \{1,\,2,\,3\}$, and can be written as:

$$\begin{cases} \phi_{p,\,1}(f) = \Delta\phi_{\mathrm{IF},\,C2}(f) - \Delta\phi_{\mathrm{IF},\,C1}(f) \\ \phi_{p,\,2}(f) = \Delta\phi_{\mathrm{IF},\,C3}(f) - \Delta\phi_{\mathrm{IF},\,C2}(f) \\ \phi_{p,\,3}(f) = \Delta\phi_{\mathrm{IF},\,C4}(f) - \Delta\phi_{\mathrm{IF},\,C3}(f) \end{cases} \tag{7}$$

where $\Delta\phi_{\mathrm{IF},\,Cj}$ represents the phase shift evaluated at the IF signal, achieved by the circuit C_j, with $j = \{1,\ldots,4\}$, when its working point is the indicated in Fig. 6(b).

The value of $\phi_{p,\,i}(f)$ has been represented in Fig. 10, together with the optimum frequency response of the phase shift for which the frequency scanning effect is compensated, when $\theta_{m,\,c} = -10°$. As can be observed, on the one hand, the variation of the phase shift along the considered frequency band is less than 0.5° (1.3 % of the center value). Thus, as was previously stated, it can be assumed to be constant. On the other hand, although all the IL3HSOM are identical, small differences between $\phi_{p,\,i}(f)$ are found, due to the fact that the four circuits work at different operating points.

In order to impose the desired frequency response of the phase shift, an optimization process in which two copies of the IL3HSOM are involved, is performed. The working points of the two circuits are selected in order to reach a phase difference between their output IF signals of $\phi_p(f = 11\,\mathrm{GHz}) \approx 43°$, which provides $\theta_{m,\,c} = -10°$

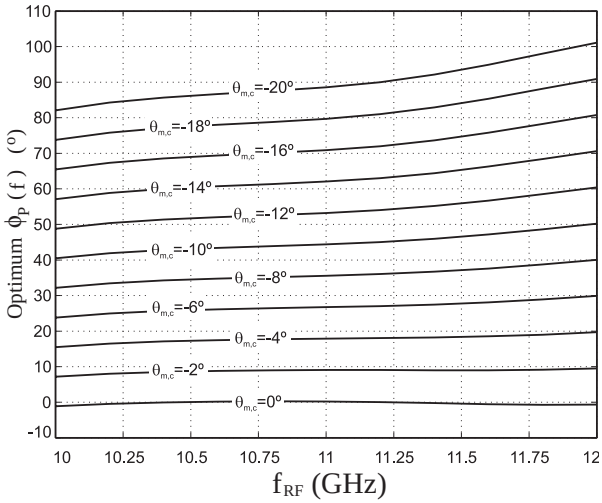

Figure 9. Optimum frequency response of $\phi_p(f)$, as a function of the value of $\theta_{m,\,c}$, at $f_{\mathrm{RF}} = 11\,\mathrm{GHz}$.

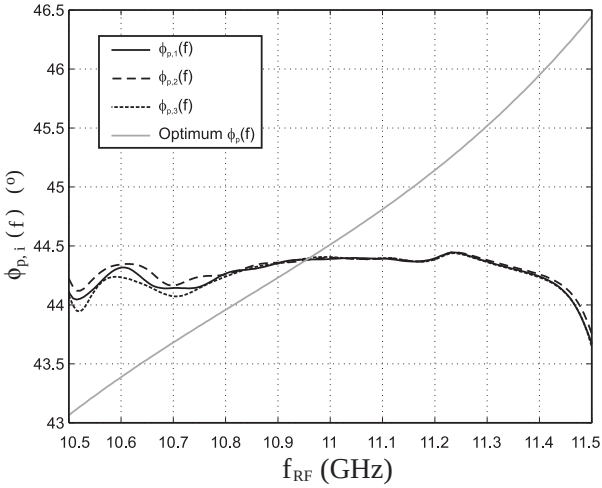

Figure 10. Frequency response of the progressive phase shift $\phi_{p,\,i}(f)$ reached between each pair of adjacent circuits, evaluated at the IF signal, before the optimization.

at $f_{\mathrm{RF}} = 11\,\mathrm{GHz}$ (see Fig. 9). Note that the two circuits share the reference signal. Hence, the frequency of their autonomous signals is identical and the only differences between them are the phases of the auxiliary generators, $\phi_{AG,\,1}$ and $\phi_{AG,\,2}$, and the value of the varactor capacities $C_{\mathrm{var},\,1}$ and $C_{\mathrm{var},\,2}$.

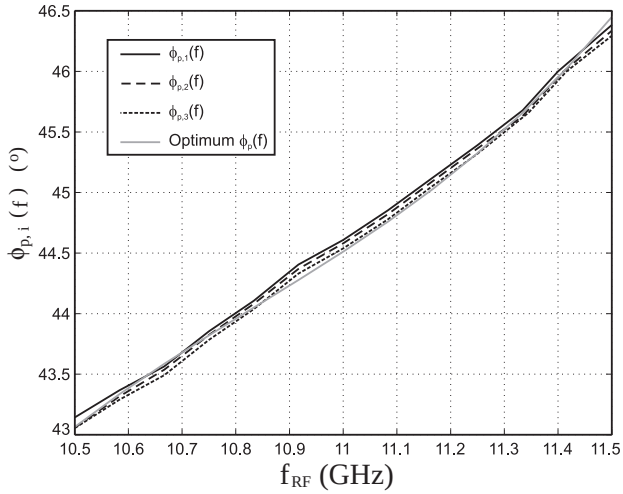

Figure 11. Frequency response of the progressive phase shift $\phi_{p,\,i}(f)$, reached between the IF signals of each pair of circuits, after the optimization process.

With the described setup, the phase difference between the two output IF signals $\phi_p(f) = \Delta\phi_{\mathrm{IF},\,2} - \Delta\phi_{\mathrm{IF},\,3}$ can be evaluated. Note that such difference is the same as $\phi_{p,\,2}(f)$ in (7). The optimum frequency response of the phase shift is imposed through an optimization process in which the parameters which define the multi-harmonic load $\bar{\gamma}_p$ are modified in order to fulfill the non perturbation condition of the two auxiliary generators while the optimum value of $\phi_p(f)$ is imposed. The optimization conditions can be written as:

$$\begin{cases} Y^r_{AG,\,1}(f_{AG,\,1},\ \phi_{AG,\,1},\ V_{AG,\,1},\ C_{\mathrm{var},\,1},\ \bar{\gamma}_p) = 0 \\ Y^i_{AG,\,1}(f_{AG,\,1},\ \phi_{AG,\,1},\ V_{AG,\,1},\ C_{\mathrm{var},\,1},\ \bar{\gamma}_p) = 0 \\ Y^r_{AG,\,2}(f_{AG,\,2},\ \phi_{AG,\,2},\ V_{AG,\,2},\ C_{\mathrm{var},\,2},\ \bar{\gamma}_p) = 0 \\ Y^i_{AG,\,2}(f_{AG,\,2},\ \phi_{AG,\,2},\ V_{AG,\,2},\ C_{\mathrm{var},\,2},\ \bar{\gamma}_p) = 0 \\ \phi_p(\bar{f},\ C_{\mathrm{var},\,1},\ C_{\mathrm{var},\,2},\ \bar{\gamma}_p)) - \phi_{p,\,g}(\bar{f}) = 0 \end{cases} \tag{8}$$

where $\phi_{p,\,g}(\bar{f})$ is the optimum frequency response of the phase shift, and $\bar{f}$ represents the set of frequency points in which the expression is evaluated.

The achieved frequency response of the phase shift $\phi_p(f)$, after the fulfillment of the conditions expressed in (8) has been represented in Fig. 11 together with its optimum value. The progressive phase

shift between the circuits C_2 and C_1, and circuits C_4 and C_3, $\phi_{p,1}$ and $\phi_{p,3}$ respectively, have also been depicted. The maximum difference between the optimum and the reached frequency responses is less than 0.15°. Note that the values of $\phi_{p,1}$ and $\phi_{p,3}$ have not been taken into account in the optimization process. However, since the four circuits are practically equal, their behavior is also very similar.

Finally, it must be taken into account that due to the autonomous nature of the phase shifter, its behavior strongly depends on the circuit load. In order to ensure the proper performance of the system, the input impedance obtained at each port of the antenna array through electromagnetic simulations has been used as load of the corresponding phase shifter during the optimization process.

4.5. Conversion Gain After the Optimization

Since the conversion gain of the circuit has not been taken into account along the optimization of $\phi_p(f)$, some changes are expected. The frequency response of the conversion gain after the optimization process is shown in Fig. 12(a), together with its previous value. The maximum value decreases about 2.5 dB, and a bandwidth reduction of 50 MHz is observed. However, the conversion gain is still over $G_c \approx 0$ dB, which is a considerably high value for a circuit based on a harmonic self-oscillating mixer.

The influence of the working point over the synchronization loci on the conversion gain has also been analyzed by calculating the difference ΔG_c between the conversion gain of each pair of adjacent circuits, when their working points are the indicated in Fig. 6(b). The result of this analysis is represented in Fig. 12(b). If the new working band, from $f_{\mathrm{RF}} = 10.55$ GHz to $f_{\mathrm{RF}} = 11.5$ GHz, shown in Fig. 12(a) is considered, the maximum conversion gain variation is less than 0.2 dB. Thus, it can be assumed that the conversion gain is almost constant along the synchronization loci. Note that the working points distribution shown in Fig. 6(b) corresponds to the worst case, since ϕ_p takes its maximum reachable value.

4.6. Compensation of the Frequency Scanning Effect

The improvement of the frequency scanning effect has been analyzed by extracting the phase values of the array feeding distribution from Fig. 11. The obtained feeding distribution has been applied to the array, and its radiation pattern has been calculated through electromagnetic simulations based on the Method of Moments. Fig. 13 represents the frequency variation of the beam-steering angle θ_m with respect to its value $\theta_{m,c}$ at the center frequency $f_{\mathrm{RF}} = 11$ GHz.

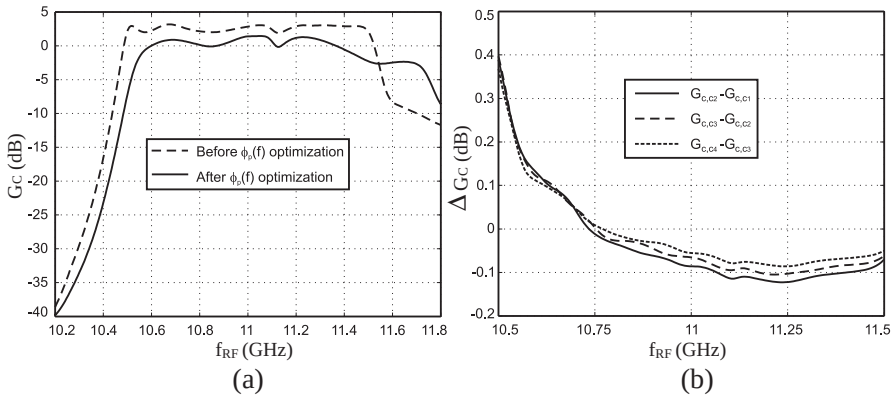

Figure 12. Conversion gain after $\phi_p(f)$ optimization. (a) Frequency response of the conversion gain. (b) Difference between the conversion gain of each pair of adjacent circuits, evaluated at $f_{\mathrm{RF}} = 11\,\mathrm{GHz}$.

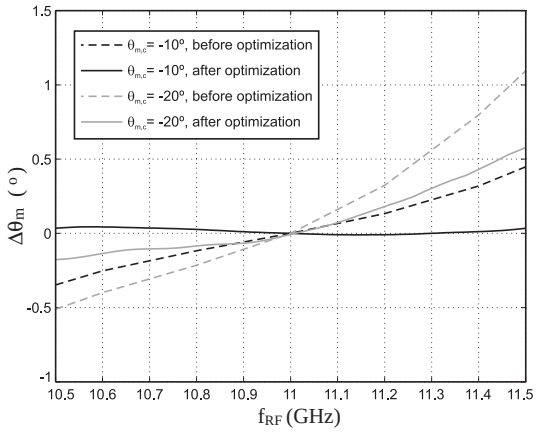

Figure 13. Frequency variation of θ_m with respect to its value at the center frequency band $\theta_{m,\,c}$. Two cases are considered: $\theta_{m,\,c} = -10°$ and $\theta_{m,\,c} = -20°$.

Two cases of $\theta_{m,\,c}$ have been considered. On the one hand, when $\theta_{m,\,c} = -10°$, the frequency scanning effect is compensated, due to the fact that the optimum frequency response of the phase shift $\phi_p(f)$ which has been calculated and imposed to the circuit, is the corresponding to that case.

On the other hand, the frequency response of the progressive phase shift mainly depends on the multi-harmonic load transfer function.

Therefore, the shape of $\phi_p(f)$ shown in Fig. 11 remains almost unchanged, regardless of its value at the center of the frequency band. Therefore, the worst considered case occurs when $\theta_{m,c} = -20°$, with $\phi_p(f = 11\,\text{GHz}) \approx 90°$, since it corresponds to the maximum frequency variation of θ_m. In this case, as can be observed in Fig. 13, the frequency scanning effect is not entirely corrected, but it is considerably reduced.

The compensation of the frequency scanning effect in all the other cases, with values of $\theta_{m,c}$ from 0° to −20° is expected to be between the two cases shown in Fig. 13. In addition, due to the symmetry of the problem, the behavior of the array with $\theta_{m,c}$ between 0° and 20° can be supposed to be equivalent to what has been described.

5. CONCLUSIONS

A broadband large range phase shifter based on an Injection-Locked Third Harmonic Self-Oscillating Mixer (IL3HSOM) has been presented. Besides phase shifting, this multifunctional circuit works as frequency down-converter, generates the local oscillator signal, and has been optimized to achieve a conversion gain greater than 0 dB over a 1 GHz bandwidth. The application of the broadband IL3HSOM to the design of phased antenna arrays has been described. The use of a multi-harmonic load based on an arbitrarily width modulated transmission line allows the development of an optimization technique in which the optimum phase shift frequency response can be imposed to the circuit, in order to minimize the impact of the frequency scanning effect on the antenna performance. The obtained results show that this phenomenon is considerably reduced and can be almost fully compensated in some particular cases.

ACKNOWLEDGMENT

This work has been supported by the "Ministerio de Ciencia e Innovación" of Spain and "FEDER", under projects IPT-2011-0951-390000 (TECNIGRAF), TEC2011-24492 (ISCAT), TEC2008-01638 (INVEMTA), "CONSOLIDER-INGENIO CSD2008-00068" (TERASENSE) and grant AP2009-0438, by the "Plan de Ciencia y Tecnología" (PCTI/FEDER-FSE) of the "Gobierno del Principado de Asturias", under projects EQUIP08-06, FC09-COF09-12, EQUIP10-31 and PC10-06, and grant BP10-031, and by the "Catedra Telefonica-Universidad de Oviedo".

REFERENCES

1. Buonanno, A. and M. D'Urso, "Large phased arrays diagnostic via distributional approach," *Progress In Electromagnetics Research*, Vol. 92, 153–166, 2009.
2. Oikonomou, A., I. S. Karanasiou, and N. K. Uzunoglu, "Phased-array near field radiometry for brain intracranial applications," *Progress In Electromagnetics Research*, Vol. 109, 354–360, 2010.
3. Harmer, S. W., S. E. Cole, N. J. Bowring, N. D. Rezgui, and D. Andrews, "On body concealed weapon detection using a phased antenna array," *Progress In Electromagnetics Research*, Vol. 124, 187–210, 2012.
4. Wang, Z. G., B. Yan, R. M. Xu, and Y. C. Guo, "Design of ku band six bit phase shifter using periodically loaded-line and switched-line with loaded-line," *Progress In Electromagnetics Research*, Vol. 76, 369–379, 2007.
5. Tahir, F. A., and H. Aubert, "Equivalent electrical circuit for designing mems-controlled reflectarray phase shifters," *Progress In Electromagnetics Research*, Vol. 100, 1–12, 2010.
6. Che, W.-Q., E. K. N. Yung, K. Wu, and X.-D. Nie, "Design investigation on millimeter-wave ferrite phase shifter in substrate integrated waveguide," *Progress In Electromagnetics Research*, Vol. 45, 263–275, 2004.
7. Moghadasi, M. N., G. Dadashzadeh, A. Dadgarpour, F. Jolani, and B. S. Virdee, "Compact ultra-wideband phase shifter," *Progress In Electromagnetics Research Letters*, Vol. 15, 89–98, 2010.
8. Daryoush, A. S., M. Francisco, R. Saedi, et al., "Phase control of optically injection locked oscillators for phased arrays," *Proceedings of the IEEE MTT-Symposium Digest*, 1247–1250, U.S.A., 1990.
9. York, R. A. and T. Itoh, "Injection and phase-locking techniques for beam control," *IEEE Transactions on Antennas and Propagation*, Vol. 46, No. 11, 1920–1929, 1998.
10. Sthephan, K. D. and W. A. Morgan, "Analysis of inter-injection-locked oscillators for integrated phased arrays," *IEEE Transactions on Antennas and Propagation*, Vol. 35, 771–781, 1987.
11. Wang, J. H. and N. H. Myung, "A new beam-scanning technique by controlling the coupling angle in a coupled oscillator array," *IEEE Microwave and Guided-Wave Letters*, Vol. 8, No. 5, 491–493, 1998.

12. Ver Hoeye, S., A. Suarez, and S. Sancho, "Analysis of noise effects on the nonlinear dynamics of synchronized oscillators," *IEEE Microwave and Wireless Components Letters*, Vol. 11, No. 9, 376–378, 2001.
13. Ver Hoeye, S., L. F. Herran, M. Fernandez, and F. Las Heras, "Design and analysis of a microwave large-range variable phase-shifter based on an injection-locked harmonic self-oscillating mixer," *IEEE Microwave and Wireless Components Letters*, Vol. 16, No. 6, 342–344, 2006.
14. Fernandez, M., S. Ver Hoeye, C. Vazquez, G. Hotopan, R. Camblor, and F. Las Heras, "Optimization of the synchronization bandwidth of rationally synchronized oscillators based on bifurcation control," *Progress In Electromagnetics Research*, Vol. 119, 299–313, 2011.
15. Ver Hoeye, S., C. Vazquez, M. Fernandez, L. F. Herran, and F. Las Heras, "Multi-harmonic dc-bias network based on arbitrarily width modulated microstrip line," *Progress In Electromagnetics Research Letters*, Vol. 11, 119–128, 2009.
16. Gonzalez-Posadas, V., J. L. Jimenez-Martin, A. Parra-Cerrada, D. Segovia-Vargas, and L. E. Garcia-Munoz, "Oscillator accurate linear analysis and design. Classic linear methods review and comments," *Progress In Electromagnetics Research*, Vol. 118, 89–116, 2011.
17. Fernandez, M., S. Ver Hoeye, C. Vazquez, G. R. Hotopan, R. Camblor, and F. Las Heras, "Design and analysis of a multi-carrier Tx-Rx system based on rationally synchronized oscillators for localization applications," *Progress In Electromagnetics Research*, Vol. 120, 1–16, 2011.
18. Fernandez, M., S. Ver Hoeye, L. F. Herran, and F. Las Heras, "Nonlinear optimization of wide-band harmonic self-oscillating mixers," *IEEE Microwave and Wireless Components Letters*, Vol. 18, No. 5, 347–349, 2008.
19. Adler, R., "A study of locking phenomena in oscillators," *IEEE Proceedings*, Vol. 61, No. 10, 1380–1385, 1973.
20. Asimakis, N. P., I. S. Karanasiou, and N. K. Uzunoglu, "Non-invasive microwave radiometric system for intracranial applications: A study using the conformal L-notch microstrip patch antenna," *Progress In Electromagnetics Research*, Vol. 117, 83–101, 2011.
21. Montero-de-Paz, J., E. Ugarte-Munoz, and F. J. Herraiz-Martinez, "Multifrequency self-diplexed single patch antennas loaded with split ring resonators," *Progress In Electromagnetics*

Research, Vol. 113, 47–66, 2011.

22. Goel, P. and K. J. Vinoy, "A low-cost phased array antenna integrated with phase shifters cofabricated on the laminate," *Progress In Electromagnetics Research B*, Vol. 30, 255–277, 2011.
23. Garcia, J. A., L. Cabria, R. Marante, L. Rizo, and A. Mediavilla, "An unbiased dual-mode mixing antenna for wireless transponders," *Progress In Electromagnetics Research*, Vol. 102, 1–14, 2010.
24. Moradi, K. and S. Nikmehr, "A dual-band dual-polarized microstrip array antenna for base stations," *Progress In Electromagnetics Research*, Vol. 123, 527–541, 2012.
25. Dahlan, A. M. M. and M. R. Kamarudin, "Shorted microstrip path antenna with parasitic element," *Journal of Electromagnetic Waves and Applications*, Vol. 24, Nos. 2–3, 327–339, 2010.
26. Zhao, K., S. Zhang, and S. L. He, "Enhance the bandwidth of a rotated rhombus slot antenna with multiple parasitic elements," *Journal of Electromagnetic Waves and Applications*, Vol. 24, Nos. 14–15, 2087–2094, 2010.
27. Mohamadi, F. and N. Komjani, "Bandwidth enhancement of microstrip pathc antenna using Jerusalem cross-shaped frequency selective surfaces by invasive weed optimization approach," *Progress In Electromagnetics Research*, Vol. 121, 103–120, 2011.
28. Zhao, X.-W., Y. Zhang, H.-W. Zhang, D. G. Donoro, S.-W. Ting, T. K. Sarkar, and C.-H. Liang, "Parallel MoM-PO method with out-of-core technique for analysis of complex arrays on electrically large platforms," *Progress In Electromagnetics Research*, Vol. 108, 1–21, 2010.